IEEE Access
Multidisciplinary | Rapid Review | Open Access Journal

Received June 26, 2019, accepted July 3, 2019, date of publication July 9, 2019, date of current version July 26, 2019.

Digital Object Identifier 10.1109/ACCESS.2019.2927464

Thermal Analysis and Experimental Validation of a 30 kW 60000 r/min High-Speed Permanent Magnet Motor With Magnetic Bearings

BAOTIAN DONG[1,3], KUN WANG[1,3], BANGCHENG HAN[1,2], AND SHIQIANG ZHENG[2,3]

[1]School of Instrumentation Science and Opto-electronics Engineering, Beihang University (BUAA), Beijing 100191, China
[2]Ningbo Institute of Technology, Beihang University (BUAA), Ningbo 315800, China
[3]Beijing Engineering Research Center of High-Speed Magnetically Suspended Motor Technology and Application, Beihang University (BUAA), Beijing 100191, China

Corresponding author: Kun Wang (wangkunggg@163.com)

This work was supported by the National Natural Science Foundation of China under Grant 61822302 and Grant 61721091.

ABSTRACT Thermal analysis calculation is an indispensable checking process in the design of the high-speed permanent magnet synchronous machine (HSPMSM) with the active magnetic bearings, due to its high loss density and non-contact support mode. The finite element method (FEM) is applied for visual global temperature distribution. Because the thermal analysis is a complex problem reflected the interaction among the electromagnetic field, temperature field, and fluid field, so it cannot be solved independently, and a multi-physical field simulation based on magneto-thermal-fluid coupled iterative solution is proposed. An electromagnetism (EM) model is established to solve electromagnetic loss and the computational fluid dynamics (CFD) software is used to simulate convective condition, both the results are applied to the thermal analysis of motor. The data interaction is bidirectional and transfers in the form of a field, and the interaction during the EM model, the CFD model, and thermal analysis is fully considered to guarantee high accuracy. Finally, two prototypes of 30-kW 60000 r/min magnetically suspended HSPMSMs have been developed. The experimental results of back-to-back towing test validate the accuracy of the proposed multi-physical field simulation.

INDEX TERMS Back-to-back motor towing experiment, cooling design, electromagnetic-thermal-fluid coupling analysis, high-speed permanent magnet motor, magnetic bearings, multi-physics analysis, thermal analysis.

I. INTRODUCTION

High-speed permanent magnet synchronous machines (HSPMSMs) have attracted much attention due to their compact size for direct-drive applications. The application of the active magnetic bearings (AMBs) overcomes the speed limitation of the mechanical bearings, which makes it possible for the motor to achieve a higher speed [1]–[3]. Because of the advantages of the HSPMSMs with the AMBs, such as high efficiency, high power density and no lubrication, magnetically suspended HSPMSMs have drawn lots of attention in the research of high-speed motor, and been widely used in the field of industrial high-speed rotation equipment [4]–[6]. However, with the increase of the power density of the high-speed PM motor, the loss density is increased significantly, and compact size means less heat dissipation area. High speed and high frequency will lead to high wind friction loss and high eddy current loss on the rotor, and the rotor is supported by AMBs with non-contact, hard to dissipate heat through heat conduction [7], [8]. If there is no additional cooling measures implemented, the operating temperature of the motor will rise sharply, which leads to a series of malfunctions including the demagnetization of the PMs, the strength reduction of the rotor, and the coil short circuit. Hence heat dissipation is a major technical challenge and before entering to the fabrication stage, an accurate thermal simulating model can satisfactorily reveal many of practical considerations [9].

Accurate simulation method of the temperature field is related to the accurate electromagnetic loss estimation and cooling medium characteristic analysis. In recent years, lots of research was reported in motor thermal analysis.

The associate editor coordinating the review of this manuscript and approving it for publication was Xiaodong Sun.

The lumped-parameter thermal network (LPTN) was first used to approximate the motor temperature field. In the thermal network, the parts with similar temperatures are seen as nodes, which are connected by heat conduction and convection. The electromagnetic loss and convection heat transfer coefficient (CHTC) are obtained by simplified mathematical models with empirical formulas and are assigned to these nodes as uniform values [10], [11]. The temperature value of these nodes can be obtained, but that is not enough to represent the details of the temperature distribution. Then 3-D finite element method (FEM) was developed to analyze electromagnetic model and thermal model [12]–[14]. Loss distributions and detailed temperature fields are acquired by dividing the solution domain into thousands of elements. In particular, the loss distribution applied to solve the temperature field, make the results close to the truth [15]–[17]. But the most limitation of the FEM solution is that the software uses empirical-based algorithms for convection boundaries, exactly as in the lumped circuit analysis [18]. As a consequence, the result accuracy is dependent on the same factors previously described for the thermal network. To replace the empirical method, computational fluid dynamics (CFD) analysis is regarded as an accurate method to solve the convection conditions [19]–[21]. The main strength of the numerical CFD approach is can be used to predict the flow in complex regions, such as around the end windings [22]. Currently, most CFD software has integrated the thermal solver and realizes the fluid-solid coupling technique to solve the temperature field of motor. In which the CHTC is not as a uniform value, but a data field to be submitted to the thermal calculation, the interaction between fluid temperature and motor temperature is also considered [23]–[25].

In addition, more attention has been paid to the interaction between electromagnetic field and thermal field [26]–[29]. It is believed that the thermal analysis is a global solution problem reflected the interaction among the electromagnetic field, temperature field and fluid field. Hence, the multi-physical field coupling analysis become necessary to get an accurate temperature field result [30], [31]. In the thermal analysis presented later, both the coupling electromagnetic–thermal analysis based on two-way multiple iterations and the coupling thermal–fluid analysis based on conjugate heat transfer are incorporated to guarantee high accuracy. The whole visible temperature field of the motor is obtained, which can clearly indicate the position and value of the highest temperature rise. The experimental data are compared with simulation results to verify the correctness of the proposed method.

II. METHODOLOGY

In electromagnetic loss analysis, the winding loss can be described briefly by

$$P_{phase} = KI^2 R_{phase}(1 + \alpha T_{coil}) \tag{1}$$

where P_{phase} is the winding loss for one phase, I is current, R_{phase} is resistance, and K is the growth factor of the resistance related to high frequency effect, α is the inherent temperature coefficient of copper indicating the change of resistance with temperature and T_{coil} is the operating temperature of the coil. That means accurate loss analysis depends on known temperature field.

In FEM thermal analysis, the element with heat source needs to solve the partial differential equation as

$$\rho c \frac{\partial T}{\partial t} = \lambda \left(\frac{\partial^2 T}{\partial x^2} + \frac{\partial^2 T}{\partial y^2} + \frac{\partial^2 T}{\partial z^2} \right) + \rho q \tag{2}$$

where ρ is density, c is specific heat, $T = T(x, y, z, t)$ is element temperature function, t means time, λ is thermal conductivity, and q is heat generation rate which needs to be provided by the results of electromagnetic loss analysis. Correspondingly, in the elements on the interface with the cooling medium, the partial differential equation to be solved as

$$\lambda \left(\frac{\partial T}{\partial x} n_x + \frac{\partial T}{\partial y} n_y + \frac{\partial T}{\partial z} n_z \right) = h(T_w - T_f) \tag{3}$$

where n_x, n_y and n_z are normal vectors, h is the CHTC on the interface, T_w is the temperature on the solid side, and T_f is the temperature of the fluid. Reliable CHTC and T_f require CFD analysis of the fluid field. Conversely, for CFD analysis, the T_w obtained from thermal analysis is also needed as a boundary condition for CFD fluid energy equation.

In conclusion, the thermal analysis requires the loss information of electromagnetic analysis and convection boundary conditions from CFD analysis. Electromagnetic analysis and CFD analysis are also affected by temperature field. They are coupled with each other and cannot be solved independently, must be solved step by step through iteration based on data interaction. In this paper, a multi-physical field coupling simulation based on magneto-thermal-fluid coupled iterative solution is established, which is applied to the temperature field analysis of a high-speed magnetically suspended PM motor with rated power of 30-kW and rated speed of 60000r/min. The coupling simulation accuracy was detected by the final back-to-back motor towing experiment.

III. CONFIGURATION

The configuration of the HSPMSMs with the AMBs is shown in Fig. 1. The component consisted of the integral structure contains motor stator, rotor, a radial AMB, a combined radial-axial magnetic bearing (CRAMB), backup bearings, water jacket, and circuit box. Some of the major parts are shown in Fig. 2. The main structure parameters are listed in Table 1.

Because the total heat loss of the motor is large, the temperature of the motor will rise sharply, if the heat cannot dissipate rapidly, which will cause the damage of the motor due to the insulation failure. Therefore, a stator jacket with water cooling was designed for a high heat dissipation efficiency as shown in Fig. 1. The cold water was supplied by an external refrigerator with 0.1MPa inlet pressure and 30°C initial temperature. Moreover, the high-speed rotation will cause the high air friction loss and the high eddy current loss on the rotor surface. Due to the non-contact support

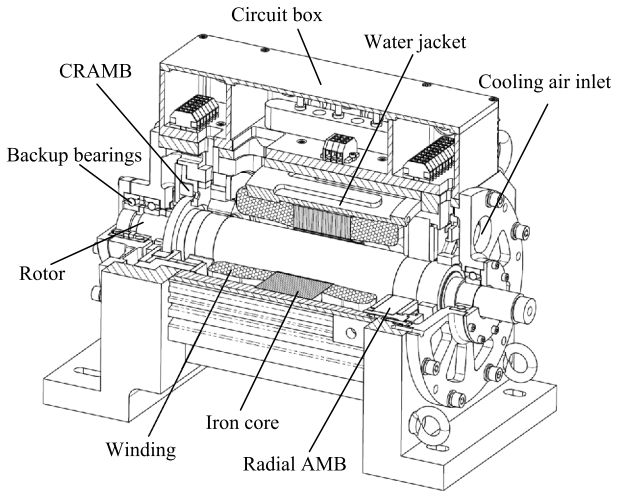

FIGURE 1. Overall configuration of the HSPMSM with the AMBs.

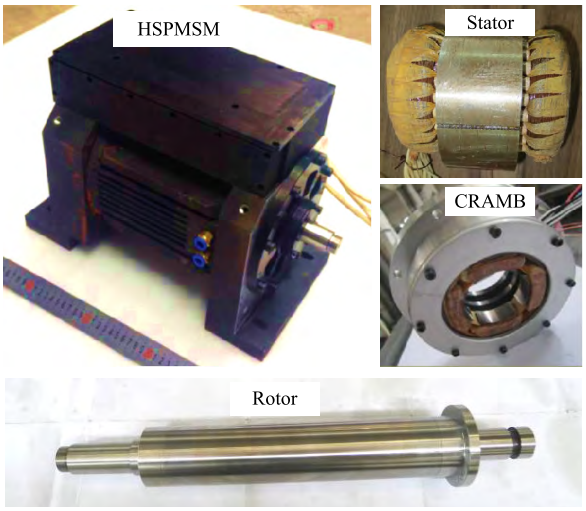

FIGURE 2. The HSPMSM and the major parts, such as stator, rotor and the CRAMB.

TABLE 1. Main motor parameters.

Parameter	Value	Parameter	Value
Rated power	30kW	Rated speed	60000r/min
Stator diameter	150mm	Stator length	60mm
Rotor diameter	55mm	Rotor length	390mm
Total quality	45kg	Total length	421mm
Total width	220mm	Total height	313mm
Water pressure	0.1MPa	Air pressure	2kPa

by AMB, the heat cannot dissipate by contact heat conduction as usual. The high temperature can cause the demagnetization of the PM in the rotor. Therefore, the forced air cooling system be adopted to enhance the air convection heat dissipation of the rotor. The cooling air inlet is arranged at the front of the prototype in Fig.1, and is cooled by an external blower of 2kPa.

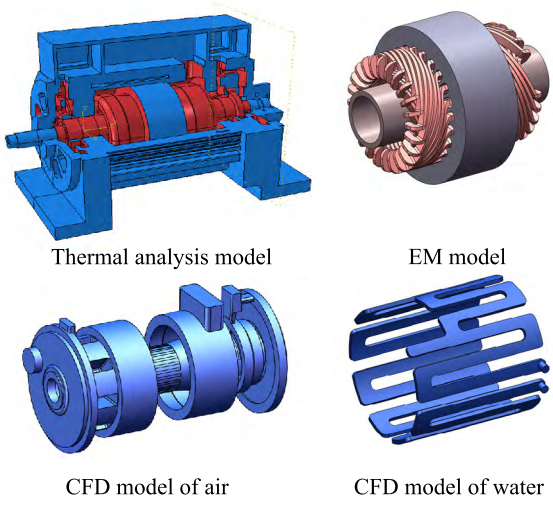

FIGURE 3. The thermal analysis model, the EM model, and the CFD models.

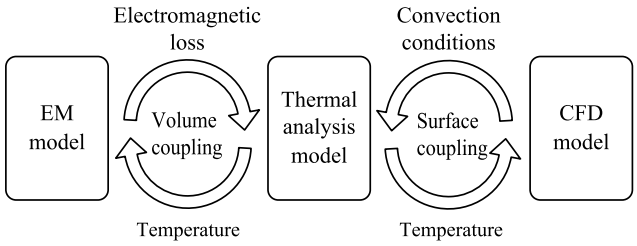

FIGURE 4. The schematic diagram of data exchange during the EM model, the thermal analysis model and the CFD models.

IV. MULTI-PHYSICS COUPLING SIMULATION

In multi-physical coupling simulation, EM model, CFD model and thermal analysis model are established by using different analysis software, and be solved iteratively by multiple analysis steps. Between iterations, the data exchange between the models is implemented by the software MPCCI (Mesh-based parallel Code Coupling Interface), so as to realize the weak coupling solution until all three models converge. Fig. 3 shows the EM model, CFD models and thermal analysis model of the prototype. First, ABAQUS is used to build the 3-D FEM thermal analysis models, including the entire motor structure. JMAG is used in the EM model of the motor to solve the iron loss in the stator and the eddy current loss in the rotor. Because the same parts of the EM model and the thermal model have the same position relative to the space coordinate system. The data exchange is easily established between the same coordinate points so that heat generation rate and temperature can be exchanged between two models. Then, two CFD models have been developed by FLUENT for the simulations of the cooling water and the cooling air system respectively. At the interface between the CFD model and thermal analysis model, a surface coupling is established to exchange convection boundary conditions and temperature. The schematic diagram of data exchange during the models is shown in Fig. 4. At the beginning, the EM model

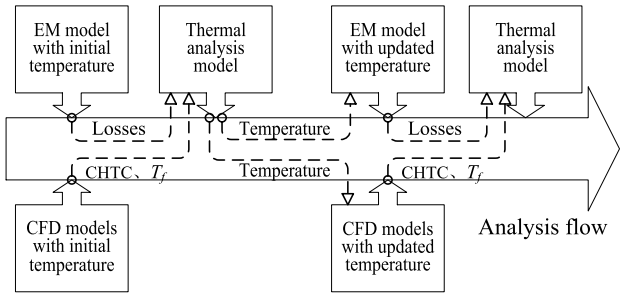

FIGURE 5. The flow chart of multi-physics coupling simulation analysis process.

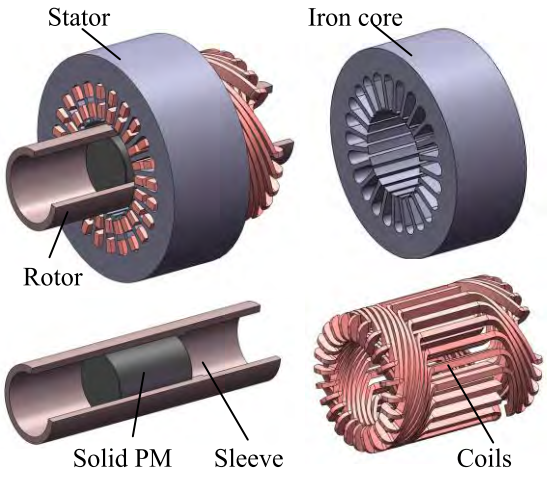

FIGURE 6. The components of the EM model.

and two CFD models are solved with an initial temperature. The EM loss and the convection conditions including CHTC and fluid temperature are obtained, which are substituted into the thermal analysis model as initial condition to solve the motor temperature field. Then the obtained temperature fields at the corresponding positions are turned back to the EM model and CFD models for next step. And so on, the multi-physics coupling simulation is iterative calculated, as illustrated in Fig. 5 until the convergence of the temperature field.

A. EM SIMULATION

As shown in Fig. 6, the EM model includes iron core, coils, and rotor. The rotor includes solid PM and sleeve, the sleeve is used to protect the permanent magnet under centrifugal load and connect other components of the rotor. The main characteristic and parameters of the EM model are shown in Table 2. The coils are connected to a three-phase sinusoidal alternating voltage source, and the amplitude is assumed to be constant. The PM rotation is defined and the initial phase of the current matches the magnetic field direction of the PM. The change of electrical conductivity with temperature is considered, whereas the change of magnetic permeability with temperature is neglected. The 3-D transient analysis is established, and the core and rotor made a volume coupled

TABLE 2. Characteristic and parameters of the EM model.

Parameter	Value
PM material	SmCo
Sleeve material	Inconel718（GH4169）
Core silicon steel sheet type	20WTG1500
Number of poles	2
Number of stator slots	24
Connection type	Y-connection
Winding type	Two layers around
Initial ac phase resistance	0.02ohm
Number of turns	6 turn
Airgap length	8 mm
Slot width	11 mm

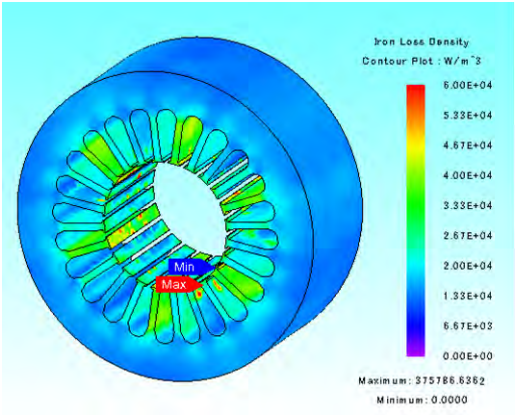

FIGURE 7. The iron loss density of core in the simulation results.

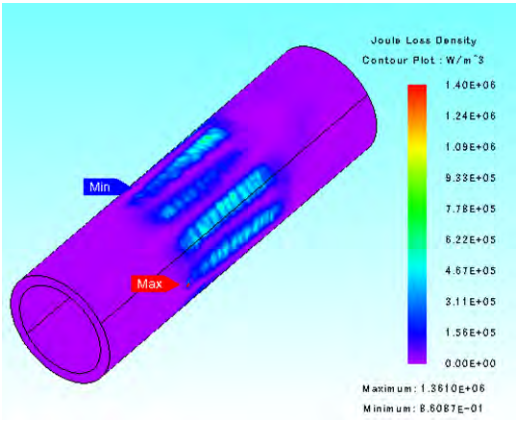

FIGURE 8. The rotor eddy current loss density of sleeve in the simulation results.

relationship with the same parts in the thermal analysis model. After each current cycle solution, the iron loss and rotor eddy current loss will be sent to the thermal analysis model. The iron loss and rotor eddy current loss in the simulation results are shown in Fig. 7and Fig. 8.

B. CFD MODEL

As shown in Fig. 3, by using Boolean operation from the thermal analysis model, two CFD models are established to

TABLE 3. Material parameters used in the CFD models.

Material parameter	Air	Water
Density	1.225kg/m^3	998.2kg/m^3
Specific heat	1006.43j/(kg·K)	4182j/(kg·K)
Conductivity	0.0242 W/(m·K)	0.6 W/(m·K)
Viscosity	1.79E-5kg/(m·s)	0.001kg/(m·s)

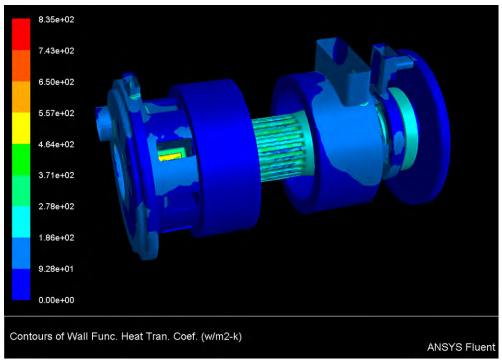

FIGURE 9. The contours of CHTC obtained at the interface between cooling air and the motor.

simulate cooling air and cooling water respectively. In the water CFD model, the laminar flow model is used, and the pressure of 0.1MPa is defined at the entrance. In the air CFD model, k-ε turbulence model is used, 2kPa entrance pressure is defined. Because air is considered as an incompressible ideal gas, so its density varies with temperature and the other properties are independent of temperature. The material parameter used in the models are briefly shown in Table 3. Rotation is defined in the interface between the cooling air and the rotor, and near air is stirred, its viscous heating is solved and used in the solution of fluid temperature field. This viscous heating is the rotor wind friction loss, can be seen as the power did by the rotor to the air. Its value can be seen from the CFD software by surface integral of the total heat transfer rate between the outlet and the inlet.

The CFD models solve independently for a fixed number steps, and then the aforementioned data exchanges are implemented at fluid-solid interfaces. Fig. 9 and Fig. 11 show the contours of CHTC obtained at the interfaces of cooling air and water. Fig. 10 shows the pressure decreases along the pathlines of cooling air. Fig. 12 shows the result of cooling water flow velocity.

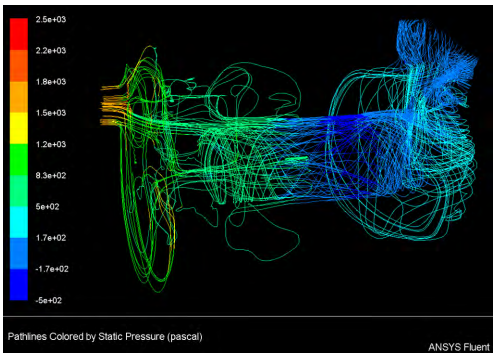

FIGURE 10. The pathlines of cooling air colored by static pressure.

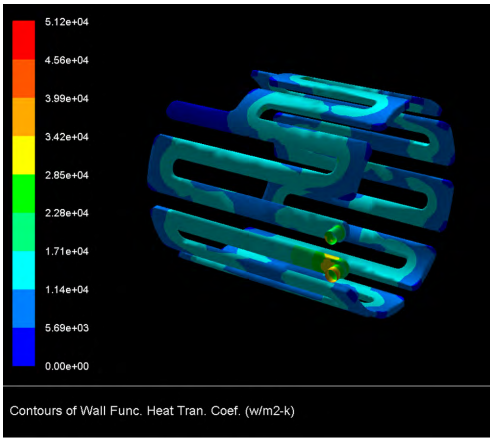

FIGURE 11. The contours of CHTC obtained at the interface between cooling water and the water jacket.

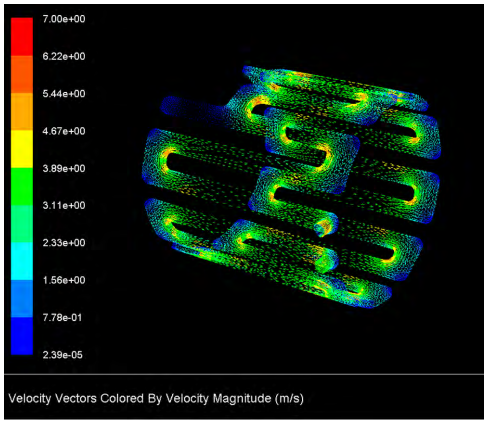

FIGURE 12. The result of cooling water flow velocity.

C. THERMAL ANALYSIS MODEL

The main heat loss of the motor includes iron loss, rotor eddy current loss, winding loss, wind friction loss and the loss of AMBs. As mentioned above, the wind friction loss is integrated in the air CFD model, and its influence through the convection at the interface to the thermal analysis model. The iron loss and rotor eddy current loss can be mapped to the thermal analysis model by volume coupling, but the winding loss cannot be mapped directly due to the different coils shapes in two models, as shown in Fig. 13. If the thermal analysis model use the coils shape in EM model, through Boolean operation, the air CFD model will be too fragmented to simulation. And the coils shape in the thermal analysis model is more close to its real situation as Fig. 2 shown. So finally, the winding loss is assumed to be uniformly distributed, and solved by empirical formulas (1) using the average coils temperature result in the last thermal

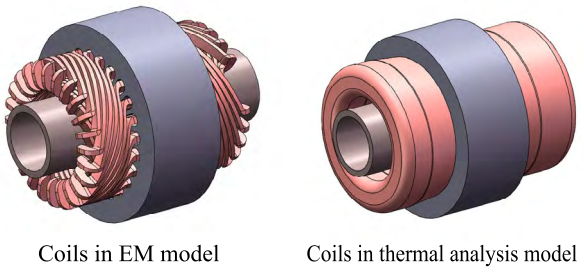

FIGURE 13. The difference in the shape of coils between the ME model and thermal analysis model.

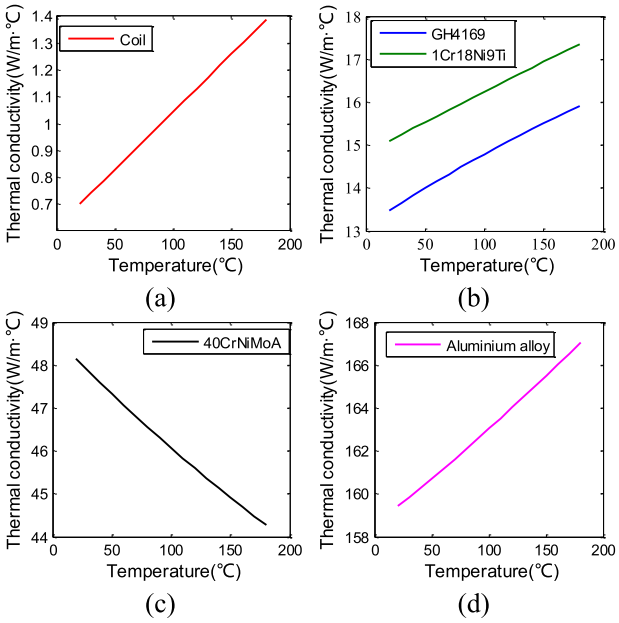

FIGURE 14. The thermal conductivity of the materials depends on temperature.

analysis step. Then the winding loss result is used to update the heat generation rate of coils for the next iteration step. Due to the current frequency is 1kHz, the resistance factor K is assigned as 1.01 to consider the influence of skin effect.

Coils are complex combinations of copper wire, insulating skin and paint, its heat conductivity can be calculated by empirical formula (4) as

$$\lambda_{coil} = 0.165(1+0.007T_{coil})\times[1-0.32d_1(1-9.2k_1+5.2k_1^2) +0.81d_1^2]\times(2.1k_2^{1.5}-0.32)(\frac{\lambda_1}{0.162})^{1\beta}(\frac{\lambda_2}{0.143})^{0.25} \quad (4)$$

where λ_{coil} is the equivalent heat conductivity of coils, T_{coil} is the coils average temperature, d_1 is the diameter of copper wire, k_1 is the winding paint coefficient, k_2 is the fill factor, λ_1 is the heat conductivity coefficient of the paint, and λ_2 is the heat conductivity of the insulating skin [31]. The calculation result is shown in Fig. 14 (a). Some other materials thermal conductivity depends on temperature is also taken into account and shown in Fig. 14, such as sleeve material (GH4169), shaft material (1Cr18Ni9Ti), AMB material (40CrNiMoA) and chassis material (aluminum alloy). Otherwise, the thermal conductivity of PM (SmCo) is set to 12W/(m·°C), the thermal conductivity of iron cores is 18W/(m·°C) in parallel direction and it is 0.55W/(m·°C) in vertical direction, their temperature dependence is neglected.

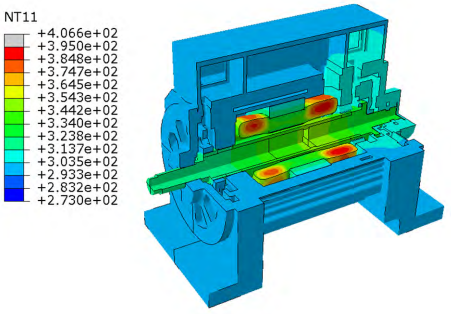

FIGURE 15. The simulation result of motor temperature field.

TABLE 4. The result of multi-physics coupling simulation.

Results	Value
Iron loss	381W
Winding loss	450W
Eddy current loss	340W
Wind friction loss	277W
Total heat loss	1367W
Mass flow rate of water	0.263kg/s
Volume flow rate of air	0.024m3/s
Temperature rise of stator core	47K
Temperature rise of rotor	50.6K
Temperature rise of cooling water	0.54K
Temperature rise of cooling air	22.97K

The heat loss of AMBs also includes iron loss and winding loss. However, compared with the loss of motor stator, the loss of AMBs is small. Actually, in the subsequent experiments, the total power consumption of AMBs in stable operation is 36W and the total loss of motor is more than 1.3kW. Because of its relatively large volume, the influence of AMBs loss on the temperature field of motor is neglected.

In this thermal analysis model, the following assumptions have also been made.

1) The PM eddy-current loss is considered to be negligible because the sleeve is thick and plays a good shielding role.

2) Radiation effect between the rotor and the stator is neglected because it has little effect on heat transfer in relatively low temperatures.

3) Define natural convection on the outer surface of the motor, with convection coefficient 5W/(m^2·°C) and constant ambient temperature 300K.

4) The contact thermal resistance between iron core and chassis is neglected because they are interference fit.

After iterative solution, the final temperature field nephogram of the motor is shown in Fig. 15. By integrating the output, we can get the loss results and temperature rise results as listed in Table 4.

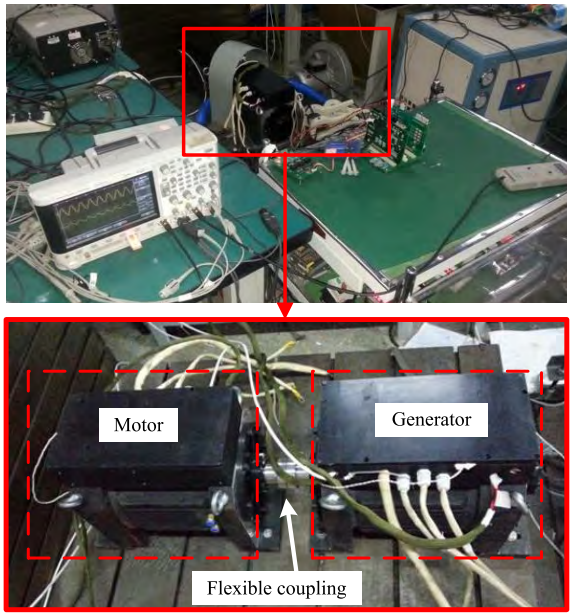

FIGURE 16. The back-to-back towing experiment of two motors.

V. EXPERIMENTAL VALIDATION

Two identical prototypes are manufactured, and the performance of the motor is tested by back-to-back towing experiments. During the experiment, one motor was used as an electric machine to drive the other motor which was used as a generator, until the motor is running stably at the rated speed 60000r/min. A flexible coupling is used to connect two shafts of them just as shown in Fig. 16. Fig. 17 illustrates the layout of the towing experiment. The motor is driven by an insulated gate bipolar transistor (IGBT) based voltage-source-inverter adjustable speed drive, and the generator is connected with a three-phase power resistance box to dissipate the energy generated. Power analyzer is used to record energy input and output. Each machine has a AMBs controller responsible for the suspension of the rotor, which controls the current and force of the AMBs according to the signal of the displacement sensor. So that the rotor shaft can be suspended in a certain range to achieve dynamic balance and an oscilloscopes is used to monitor the radial position of rotor. Due to the residual unbalanced mass of rotor, when the rotor rotates, the axis trajectory is an approximate circle. So the rotor displacement signal detected by the radial displacement sensor is an approximate sinusoidal signal, and its frequency is the same as that of rotor rotation. Actually, due to the influence of AMBs active control, there are still some clutter and interference in the sensor signal. The signal of the radial displacement sensor with the frequency of 1000 Hz is shown in Fig. 18, which means that the rotor reached the rated speed 60000r/min. The four curves on the oscilloscope represent the displacement of the rotor at the AMBs on both sides, along x-axis and y-axis respectively. And the amplitudes express the vibration range of the rotor shaft, by conversion, the maximum amplitude of vibration shown on oscilloscope is 32 μm.

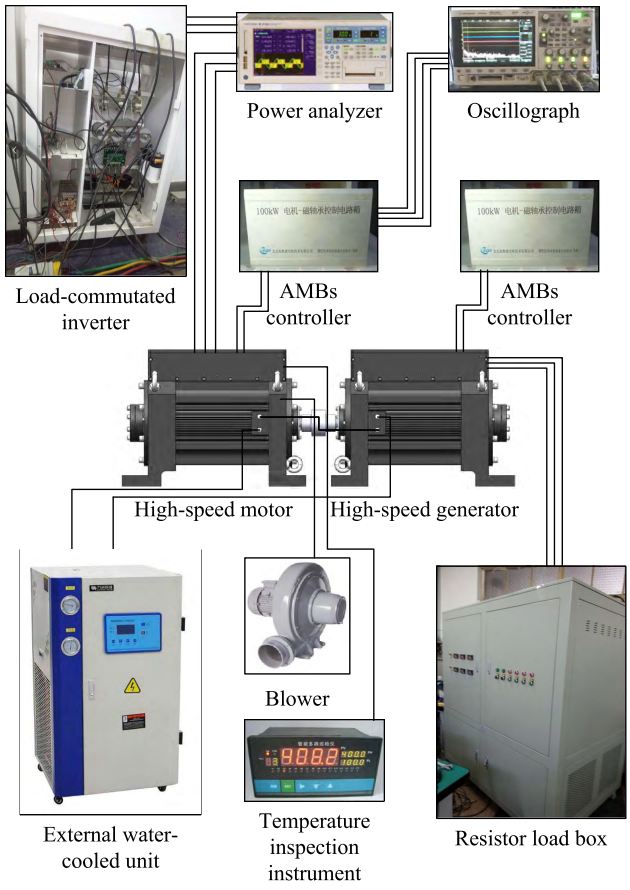

FIGURE 17. The layout of the back-to-back towing experiment.

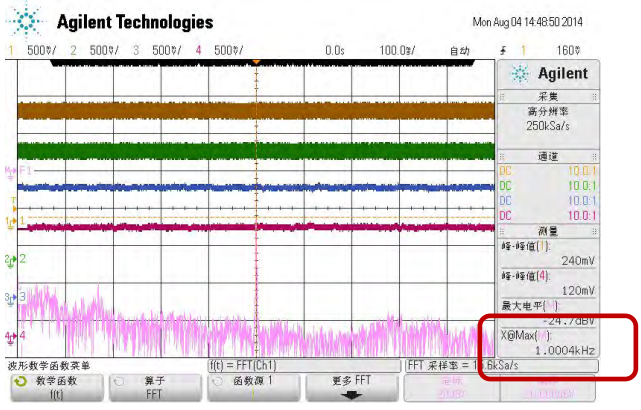

FIGURE 18. The signal of radial displacement sensor.

An external water-cooled unit with heat exchanger is used to supply constant 20°C water with 0.1MPa, and a blower is used to provide the pressure 2kPa required to force air cooling. Temperature values were measured by the thermistors (PT100) embedded in the motor stator. The positions of the thermistors embedded are marked in Fig. 19 and their positions are described below.

1) Mark 1 is in the outlet of the core slot.
2) Mark 2 is in the midpoint of the core slot.

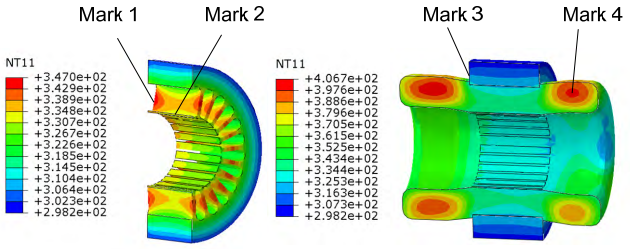

FIGURE 19. The temperature field of stator and the positions of the thermistors embedded.

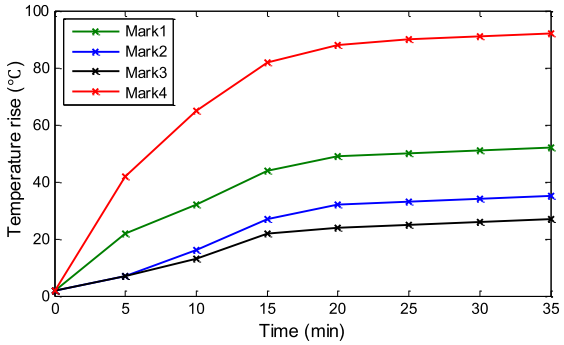

FIGURE 20. The temperature rise of the thermistors before thermal steady-state.

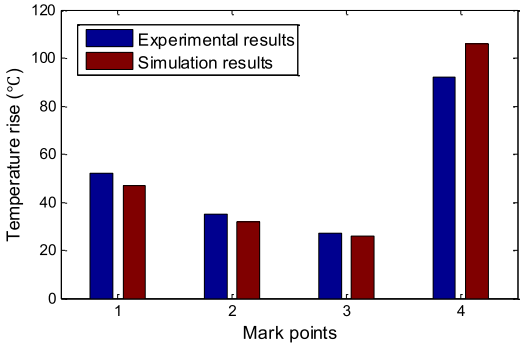

FIGURE 21. Comparison between experimental results and calculated results.

3) Mark 3 is on the end face of iron core.

4) Mark 4 is at the center of the end windings.

Fig. 19 also shows the simulation result of the motor stator temperature field. The temperature rise of the thermistors after starting is recorded by a temperature inspection instrument until thermal steady-state, and the results are shown in Fig. 20. By comparing the thermal steady-state temperature rise with the simulation result, the accuracy of the calculation method is determined as Fig. 21 shown. The results of the multi-physical field coupling simulation reach a well agreement with the experimental results, which demonstrated the accuracy of the simulation method, and this method can be applied in the subsequent design.

VI. CONCLUSIONS

The prototypes of HSPMSM supported by AMBs have been designed and fabricated. Because of its characteristics, such as high loss density, high rotational speed, non-contact support, heat dissipation become a great challenge in considerations. Therefore, it is necessary to estimate the temperature field before entering to the fabrication stage, so as to avoid the temperature accumulation leading to excessive temperature rise and failure. An accurate temperature field calculation method based on the multi-physics field coupling solution was presented, in which the main heat loss and convective conditions were solved by FEM and CFD method with less empirical formula. The effect of temperature on material electro conductibility and the temperature gradient of the fluid were taken into account. Finally, a temperature field visualization of the entire motor is obtained, it is clearly revealed that the position and value of the highest temperature rise. Compared with the experimental results from back-to-back towing experiment, the maximum error of simulation results is less than 15%, which proved the effectiveness of the multi-physics field coupling simulation. The simulation model does not depend on empirical formulas, can adapt to the changes of different structural shapes, and can be used as a reference for the further motor design.

REFERENCES

[1] B. Dong, K. Wang, B. Han, and S. Zheng, "High-speed permanent magnet motor with magnetic bearings: Multi-physics analysis, cooling design and experiment," in *Proc. Int. Conf. Elect. Mach. Syst.*, Nov. 2016, pp. 1–4.

[2] D. Gerada, A. Mebarki, N. L. Brown, C. Gerada, A. Cavagnino, and A. Boglietti, "High-speed electrical machines: Technologies, trends, and developments," *IEEE Trans. Ind. Electron.*, vol. 61, no. 6, pp. 2946–2959, Jun. 2014.

[3] A. Tenconi, S. Vaschetto, and A. Vigliani, "Electrical machines for high-speed applications: Design considerations and tradeoffs," *IEEE Trans. Ind. Electron.*, vol. 61, no. 6, pp. 3022–3029, Jun. 2014.

[4] X. Sun, B. Su, L. Chen, Z. Yang, X. Xu, and Z. Shi, "Precise control of a four degree-of-freedom permanent magnet biased active magnetic bearing system in a magnetically suspended direct-driven spindle using neural network inverse scheme," *Mech. Syst. Signal Process.*, vol. 88, pp. 36–48, May 2017.

[5] S. Zheng, B. Han, and L. Guo, "Composite hierarchical antidisturbance control for magnetic bearing system subject to multiple external disturbances," *IEEE Trans. Ind. Electron.*, vol. 61, no. 12, pp. 7004–7012, Dec. 2014.

[6] X. Sun, Z. Jin, S. Wang, Z. Yang, K. Li, Y. Fan, and L. Chen, "Performance improvement of torque and suspension force for a novel five-phase BFSPM machine for flywheel energy storage systems," *IEEE Trans. Appl. Supercond.*, vol. 29, no. 2, Mar. 2019, Art. no. 0601505.

[7] J. Shen, X. Qin, and Y. Wang, "High-speed permanent magnet electrical machines—Applications, key issues and challenges," *CES Trans. Elect. Mach. Syst.*, vol. 2, no. 1, pp. 23–33, Mar. 2018.

[8] N. Zhao and W. Liu, "Loss calculation and thermal analysis of surface-mounted PM motor and interior PM motor," *IEEE Trans. Magn.*, vol. 51, no. 11, pp. 1–4, Nov. 2015.

[9] M. Naseh and H. Heydari, "Thermo-electromagnetic analysis of radial HTS magnetic bearings using a semi-analytical method," *IET Electr. Power Appl.*, vol. 11, no. 9, pp. 1538–1547, Nov. 2017.

[10] A. Boglietti, A. Cavagnino, and D. Staton, "Determination of critical parameters in electrical machine thermal models," *IEEE Trans. Ind. Appl.*, vol. 44, no. 4, pp. 1150–1159, Jul. 2008.

[11] D. A. Staton and A. Cavagnino, "Convection heat transfer and flow calculations suitable for electric machines thermal models," *IEEE Trans. Ind. Electron.*, vol. 55, no. 10, pp. 3509–3516, Oct. 2008.

[12] Y. Liang, X. Bian, H. Yu, and C. Li, "Finite-element evaluation and eddy-current loss decrease in stator end metallic parts of a large double-canned induction motor," *IEEE Trans. Ind. Electron.*, vol. 62, no. 11, pp. 6779–6785, Nov. 2015.

[13] J. Wang, F. Wang, and X. Kong, "Losses and thermal analysis of high speed PM machine," in *Proc. Joint Int. Conf. Power Syst. Technol. IEEE Power India Conf.*, Oct. 2008, pp. 1–5.
[14] W. Jiang and T. M. Jahns, "Coupled electromagnetic–thermal analysis of electric machines including transient operation based on finite-element techniques," *IEEE Trans. Ind. Appl.*, vol. 51, no. 2, pp. 1880–1889, Mar./Apr. 2015.
[15] D. Joo, J.-H. Cho, K. Woo, B.-T. Kim, and D.-K. Kim, "Electromagnetic field and thermal linked analysis of interior permanent-magnet synchronous motor for agricultural electric vehicle," *IEEE Trans. Magn.*, vol. 47, no. 10, pp. 4242–4245, Oct. 2011.
[16] S.-T. Lee, H.-J. Kim, J.-H. Cho, D.-S. Joo, and D. K. Kim, "Thermal analysis of interior permanent-magnet synchronous motor by electromagnetic field-thermal linked analysis," *J. Elect. Eng. Technol.*, vol. 7, pp. 905–910, Nov. 2012.
[17] G. Li, J. Ojeda, E. Hoang, M. Gabsi, and M. Lecrivain, "Thermal–electromagnetic analysis for driving cycles of embedded flux-switching permanent-magnet motors," *IEEE Trans. Veh. Technol.*, vol. 61, pp. 140–151, Jan. 2012.
[18] A. Boglietti, A. Cavagnino, D. Staton, M. Shanel, M. Müeller, and C. Mejuto, "Evolution and modern approaches for thermal analysis of electrical machines," *IEEE Trans. Ind. Electron.*, vol. 56, no. 3, pp. 871–882, Mar. 2009.
[19] J. Dong, Y. Huang, L. Jin, H. Lin, and H. Yang, "Thermal optimization of a high-speed permanent magnet motor," *IEEE Trans. Magn.*, vol. 50, no. 2, pp. 749–752, Feb. 2014.
[20] J. F. Trigeol, Y. Bertin, and P. Lagonotte, "Thermal modeling of an induction machine through the association of two numerical approaches," *IEEE Trans. Energy Convers.*, vol. 21, no. 2, pp. 314–323, Jun. 2006.
[21] Y. Zhang, S. Mcloone, W. Cao, F. Qiu, and C. Gerada, "Power loss and thermal analysis of a MW high-speed permanent magnet synchronous machine," *IEEE Trans. Energy Convers.*, vol. 32, no. 4, pp. 1468–1478, Dec. 2017.
[22] C. Jungreuthmayer, T. Bauml, O. Winter, M. Ganchev, H. Kapeller, A. Haumer, and C. Kral, "A detailed heat and fluid flow analysis of an internal permanent magnet synchronous machine by means of computational fluid dynamics," *IEEE Trans. Ind. Electron.*, vol. 59, no. 12, pp. 4568–4578, Dec. 2012.
[23] J. Dong, Y. Huang, L. Jin, B. Guo, H. Lin, J. Dong, M. Cheng, and H. Yang, "Electromagnetic and thermal analysis of open-circuit air cooled high-speed permanent magnet machines with gramme ring windings," *IEEE Trans. Magn.*, vol. 50, no. 11, Nov. 2014, Art. no. 8104004.
[24] Z. Kolondzovski, A. Belahcen, and A. Arkkio, "Multiphysics thermal design of a high-speed permanent-magnet machine," *Appl. Therm. Eng.*, vol. 29, pp. 2693–2700, Sep. 2009.
[25] T. Li, Y. Fang, J. Ma, S. Liang, and C. Shi, "Optimization of motor heat dissipation systems based on three dimensional flow field analysis," in *Proc. 18th Int. Conf. Elect. Mach. Syst.*, Oct. 2015, pp. 1752–1756.
[26] H. Vansompel, A. Rasekh, A. Hemeida, J. Vierendeels, and P. Sergeant, "Coupled electromagnetic and thermal analysis of an axial flux PM machine," *IEEE Trans. Magn.*, vol. 51, no. 11, Nov. 2015, Art. no. 8108104.
[27] J. Fang, S. Zheng, and B. Han, "AMB vibration control for structural resonance of double-gimbal control moment gyro with high-speed magnetically suspended rotor," *IEEE/ASME Trans. Mechatronics*, vol. 18, no. 1, pp. 32–43, Feb. 2013.
[28] L. Alberti and N. Bianchi, "A coupled thermal–electromagnetic analysis for a rapid and accurate prediction of IM performance," *IEEE Trans. Ind. Electron.*, vol. 55, no. 10, pp. 3575–3582, Oct. 2008.
[29] P. K. Vong and D. Rodger, "Coupled electromagnetic-thermal modeling of electrical machines," *IEEE Trans. Magn.*, vol. 39, no. 3, pp. 1614–1617, May 2003.
[30] D. Gerada, A. Mebarki, N. L. Brown, K. J. Bradley, and C. Gerada, "Design aspects of high-speed high-power-density laminated-rotor induction machines," *IEEE Trans. Ind. Appl.*, vol. 58, no. 9, pp. 4039–4047, Sep. 2011.
[31] H. Guo, Z. Lv, Z. Wu, and B. Wei, "Multi-physics design of a novel turbine permanent magnet generator used for downhole high-pressure high-temperature environment," *IET Electr. Power Appl.*, vol. 7, no. 3, pp. 214–222, Mar. 2013.

BAOTIAN DONG received the B.S. and M.S. degrees in mechanical engineering from Shandong University, Jinan, China, in 2009 and 2012, respectively. He is currently pursuing the Ph.D. degree in instrumentation science and optoelectronics engineering with the Beihang University (BUAA), Beijing, China. His research interests include high-speed permanent-magnet electrical machine structural design and thermal analysis.

KUN WANG received the M.Sc. and Ph.D. degrees from the School of Mechanical Engineering and Automation, Robotics Institute, Beihang University, Beijing, China, in 2007 and 2010, respectively. He is currently a Postdoctoral Researcher with the Science and Technology on Inertial Laboratory, the Fundamental Science on Novel Inertial Instrument and Navigation System Technology Laboratory, and the School of Instrument Science and Opto-Electronics Engineering, Beihang University. His current research interests include wall-climbing robots, vibrating suction method, and magnetic levitation technology.

BANGCHENG HAN (M'16) was born in 1974. He received the M.S. degree in mechanical design and theory from Jilin University, Changchun, China, in 2001, and the Ph.D. degree in mechanical manufacturing and automation from the Changchun Institute of Optics, Fine Mechanics and Physics, Chinese Academy of Sciences, in 2004.

In 2004, he was a Postdoctoral Research Fellow with the School of Instrumentation Science and Optoelectronics Engineering, Beijing University of Aeronautics and Astronautics, Beijing, China. In 2006, he joined Beihang University (BUAA), where he is currently a Professor with the School of Instrumentation Science and Optoelectronics Engineering. He has more than 100 journal and conference publications. His research interests include mechatronics, magnetic suspension technology, and attitude control actuator of spacecraft.

SHIQIANG ZHENG was born in Shandong, China, in 1981. He received the B.S. degree from Northeast Forestry University, Harbin, China, in 2004, and the Ph.D. degree in electrical and electronics engineering from the Beihang University (BUAA), Beijing, China, in 2011, where he is currently with the School of Instrumentation Science and Optoelectronics Engineering. His main research interests include the magnetic bearing technology in the high-speed rotating machineries and attitude control actuators of spacecrafts.